GEOPHYSICAL RESEARCH LETTERS, VOL. 24, NO.11, PAGES 1319-1322, JUNE 1, 1997

Climate during glaciation and deglaciation identified through chemical tracers in ice-cores

Nigel D. Marsh and Peter D. Ditlevsen

Department of Geophysics, Niels Bohr Institute, University of Copenhagen, Denmark

Abstract. Presented here are the results and interpretations of an analysis of 8 chemical species obtained from the Greenland Ice Sheet Project 2 (GISP2) [*Mayewski et al* 1994; *Mayewski et al* 1993] ice-core, covering the period 41 - 0 Kyr BP. A reduction of the system to three distinct base vectors describing the 8 dimensional species space is possible. These are believed to represent the different sources of aerosols that have been transported via the atmosphere, and precipitated onto the Greenland ice-sheet. Physical reasoning suggests that these are mainly a signature of (1) an ocean source, (2) continental land and exposed continental shelves, and (3) biochemical land sources. Correlations between the resulting time series, describing the temporal contributions from the 3 source areas, reveal five distinct periods over the 41 Kyrs record, each differing dramatically in the contributed abundance of chemical species from the sources. Mechanisms are proposed to explain differences in the climate dynamics over the five periods, with interpretations leading to new information regarding paleo sea level and glacial extent. Such findings are important for reconstructing the climate prior to the Last Glacial Maximum (LGM).

1. Introduction

The $\delta^{18}O$ isotopic composition, obtained as a climate proxy from the Greenland ice-cores, reveals major changes in climate during the last glacial cycle [*Dansgaard et al* 1993; *GRIP members* 1993; *Grootes et al* 1993; *Stuiver et al* 1995]. The most prominent events being rapid transitions from periods of cold stadials to warmer inter-stadials during the Wisconsin (90-10 Kyr BP), which are absent in the present Holocene climate (10-0 Kyr BP). These Dansgaard/Oeschger and Heinrich events [*Dansgaard et al* 1993; *Heinrich* 1988] are also observed in ocean sediment cores as ice rafted debris [*Bond & Lotti* 1995], and have been related to the surging of glacial ice-caps with a time-scale of 2-3 Kyrs. The areal extent of ice-caps during the LGM, around 20 Kyr BP, and their subsequent deglaciation have been reconstructed from geological records, relative sea level data and model studies [*CLIMAP Project Members* 1976; *Peltier* 1994]. Very little is known about paleo sea levels and glaciation before the LGM.

Changes in the generic source areas of chemical species depend on, among others; sea level changes [*Bond & Lotti* 1995], changes in vegetation (desertification), and glacial extent [*Hammer et al* 1985] all of which have typical time-scales of several hundred years. Variations in atmospheric transport on the other hand, take place at much faster time-scales. Although studies with data from the Renland ice-core [*Hansson* 1994] suggest that observed increases in concentrations can be explained by variations in atmospheric transit and residence times alone, it is not yet possible to distinguish between effects resulting from changes in source area strength and transport processes [*Bales & Wolff* 1995]. However, it is believed that variations at time scales greater than 200 yrs are a result of source area effects and large scale changes in the atmospheric circulation [*Marsh & Ditlevsen* 1996], thus we analyse the 200 yrs mean of these signals providing 206 points for the fluxes of each of the 8 measured ions; Cl^- Na^+, K^+, Ca^{2+}, Mg^{2+}, SO_4^{2-}, NH_4^+, NO_3^-, covering the last 41 Kyrs. The measured ion concentrations are converted to fluxes using the empirical relationship between snow accumulation and $\delta^{18}O$; $Acc. = 0.23exp(0.14(\delta+35.2))$ meters ice per year [*Dansgaard et al* 1993]. The flux is then given as; $Flux = Acc. \times concentration$ since wet deposition dominates [*Wolff* 1993]. Contributions resulting from volcanic activity [*Clausen et al* 1993], extra terrestrial material etc. occur at time scales much shorter than 200 yrs and with magnitudes that will be smoothed out into the noise level at this resolution.

2. Three Source Types

In the analyses we make the following assumption; chemical tracers originate from n different source types, each of which has a constant relative abundance between the different species over the whole time series. The measured flux, $c^\alpha(t)$, for a given species $\alpha = 1, \nu$, is then, $c^\alpha(t) = \sum_i a_i(t) x_i^\alpha + \eta^\alpha(t)$, where $x_i^\alpha > 0$ represents the relative abundance of species α in source i ($\sum_\alpha (x_i^\alpha)^2 = 1$), $a_i(t) \geq 0$ is the load from source i at time t, $\eta^\alpha(t)$ is an independent noise term accounting for contributions not originating from any of the n predominant sources.

To be able to retain information regarding the dominant source types we must necessarily have $n \leq \nu$. Values of the individual species concentrations, $c^\alpha(t)$, can be thought of as lying within a ray spanned by the n

Paper number 97GL00706.
0094-8534/97/97GL-00706$05.00

vectors, x_i^α, in the ν dimensional space. The number of predominant source types, n, can then be determined from an embedding analysis using the scaling relation $N(r) \sim r^n$ where $N(r)$ is the average number of points within a sphere centered at a data point. To prevent the over domination of one species due to absolute values, they have all been normalised with respect to their individual averages. Figure 1(a) reveals the result of the embedding analysis, where the line with a slope of 3 indicates that there are 3 predominant sources. Deviations from this linear slope as r increases , is an effect due to the points being situated within a narrow ray, which at larger scales appear to be lower dimensional.

To estimate the 3 vectors, x_i^α, we performed an error minimization combined with an optimal best fit to the actual data, such that the angles between the vectors and the number of points falling outside the ray spanned by the vectors is minimized. The resulting vectors are displayed in table I.

As an independent check the analysis was repeated assuming 1-8 sources with least square fit errors plotted in figure 1(b) as a function of the number of sources. This clearly confirms that there are three predominant sources.

3. The Correlation between sources

By considering possible source areas for the 8 species and observing the dominant chemical components in each vector, a physical interpretation of the 3 source vectors representing source types; ocean, continental and bio-chemical has been made [*Ditlevsen & Marsh* 1996]. The vectors will not represent pure sources but be mixed with contributions from other source types and correlated through the atmospheric transport.

The continental vector though dominated by terrestrial dust, contains substantial chemical components associated with sea water and possessing ratio's similar to those seen in the ocean vector [*Holland* 1978]. This could be the result of two processes; i) air transporting terrestrial dust takes a path or mixes with air that passes over an ocean source area or, ii) the dust originates from newly exposed continental shelves which are rich in sea salt.

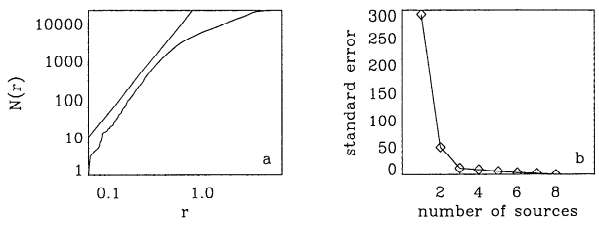

Figure 1. (a) Embedding analysis of the data in 8 dimensional space spanned by the 8 chemical species, where the values are normalised to the same mean. On a log-log scale the relation $N(r) \sim r^d$ is a straight line with slope d. This would correspond to the points being situated on a d-dimensional manifold embedded in the 8 dimensional space. The straight line has a slope of 3. (b) The standard error in fitting the 8 series, depending on the number of different source types assumed. This strongly suggests that there are 3 predominant sources.

Table 1. Source vectors obtained from GISP data

species	ocean	continental	bio-chemical
Cl^-	4.03 (0.53)	1.86 (0.25)	0.87 (0.11)
Na^+	2.25 (0.55)	1.09 (0.26)	0.21 (0.05)
K^+	0.18 (0.33)	0.19 (0.36)	0.07 (0.13)
Ca^{2+}	0.49 (0.03)	10.52 (0.66)	0.14 (0.01)
Mg^{2+}	0.52 (0.30)	0.79 (0.45)	0.07 (0.04)
SO_4^{2-}	6.76 (0.37)	5.43 (0.30)	3.14 (0.17)
NH_4^+	0.06 (0.06)	0.11 (0.10)	0.91 (0.79)
NO_3^-	3.37 (0.28)	0.99 (0.08)	6.87 (0.56)

The three source vectors for the relative abundance of each species in absolute values with units $10^{-3} gm/m^2 yr$. Values in parenthesis are the normalised vector components.

The correlation profiles between the three time series (figures 2(a-c)) with a 5400 yrs running window, are shown in figures 2(e-g). The cross-correlation between the ocean and the continental source (figure 2(e)) reveals 5 distinct temporal regions which we have indicated accordingly. (Anti-)correlations obtained between the individual signals and $\delta^{18}O$ (figure 2(d)) with the same running window signifies the nature of dependence on temperature of the source areas efficiency [*Johnsen et al* 1989; *Dansgaard et al* 1989], figures 2(h-j).

Region 5 (41-32.5 Kyrs BP) displays a strong correlation between loads from ocean and continental sources. Possibly through an atmospheric flow involving the mixing of continental and maritime air masses which are then transported as one to Greenland. Significant negative correlations of both coefficient time series with $\delta^{18}O$ indicates more efficient transportation during colder periods as a result of the increased global 'storminess' and drier conditions. Since the glaciers are yet to have expanded fully, it is possible that a major component of the continental source originated from North America as it does today. Air parcels originating over North America could pass over the Atlantic before reaching Greenland, collecting components from an ocean source en-route. The ocean time series then describes the excess ocean source not captured in the continental vector, though it is not possible to distinguish if the continental vector's ocean components are from a geographically different source area to those of the ocean vector.

The negative correlation between the ocean and continental time series during region 4 (32.5-21 Kyrs BP) is the major result of this analysis. This is difficult to explain as a consequence of increased atmospheric loading from areas such as the Gobi desert. Biscaye et al [*Biscaye et al* 1996], from isotopic experiments, has proposed that this was a substantial source area during LGM. The transport path from this region to Greenland would have to pass over the Pacific ocean and thus a correlated uptake from the ocean would be possible and could explain the lack of excess ocean source during periods of high dust. If the Gobi desert is the dominant 'pure' continental source during this period, then the

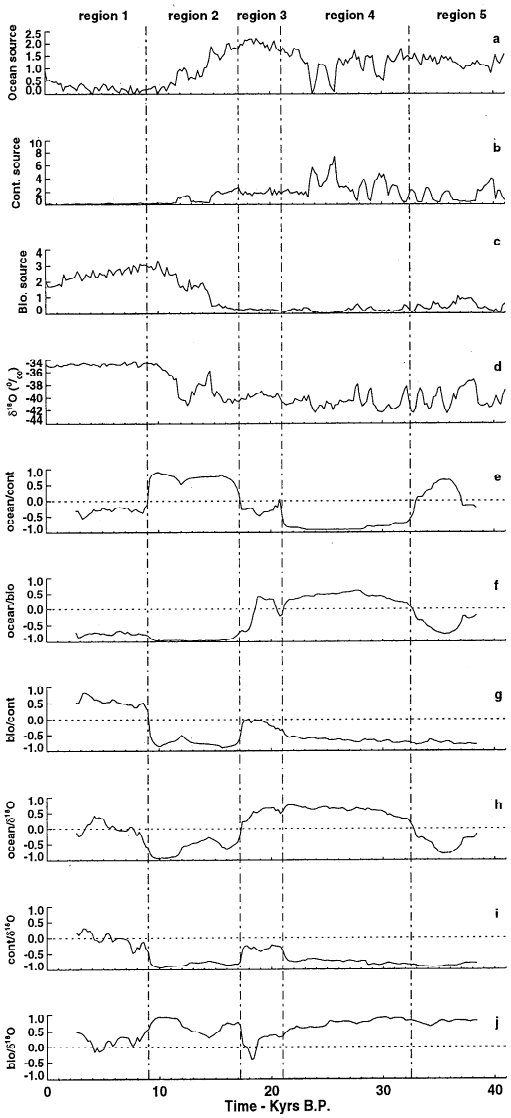

Figure 2. Coefficient timeseries for the 3 predominant source vectors **(a-c)**, and the 200 yrs mean $\delta^{18}O$ [*Meese et al* 1994] **(d)** climate record showing rapid changes in temperature during glacial times. Temporal correlations between the 4 series are taken within a running window of 5.4 Kyrs **(e-j)**. The length of the running window is selected as an optimization between statistical significance and resolving rapid changes in the temporal correlations.

continental time series acts as a tag for an ocean source originating from the Pacific ocean, while the ocean time series describes contributions from the North Atlantic. An alternative explanation for the extreme high magnitudes of continental source, could be that it originates from a more localised, high latitude source area, possibly uncovered sea shelves. A dynamical mechanism to explain the emergence of such a source and its correlation with the ocean components is proposed in the next section.

At the time of the LGM region 3 (21-17 Kyrs BP), correlations between all sources vanish. The maintenance of high values in the ocean signal, (originating from either the Pacific or lower latitudes of the North Atlantic due to extensive sea ice cover), suggests that transport in this period has strengthened, possibly due to an increased meridional temperature gradient. With the expansion of the polar cell, mixing is now at maximum strength washing out any correlations between source areas, thus no air path appears to dominate.

Region 2 covers the period of deglaciation and the Younger Dryas, during which there are strong positive correlations between ocean and continental signals, and negative temperature correlations similar to those characterising region 5.

In the Holocene period (region 1) the present day climatology is seen.

4. A Proposed Mechanism

The scatter diagram of figure 3 reveals some of the obvious changes in dynamical relationships between the ocean and continental time-series. The most striking result is that region 4 (filled dots) clearly stands out as being governed by quite different climate dynamics than during any of the other regions. Two regimes have been highlighted with straight lines, one with negative correlation corresponding to region 4, and one with weak or positive correlations for all other regions. It is during region 4 that the presence of new high latitude source areas has been postulated. As a possible explanation for this finding we propose the following mechanism.

During region 4 sea level had fallen to a level equivalent to the depth of regions such as the Bering Straits today, figure 4(a), thus new continental shelves were emerging. Periods of rapid warming (inter-stadials) coincide with ice-surging events, leading to sea level rises which could flood exposed continental shelves and cut them off as potential source areas of continental aerosol. At the same time the ocean source would increase. The result would be anti-correlation between loads from the ocean source and those from the continental source. Prior to this period (region 5) the continental shelves were not exposed, even during the colder stadials as glaciation was not near its maximum and any ice-surge events had no impact on the continental shelf source. Around the LGM (region 3) however, the sea level would have fallen to well below the exposed continental shelves, thus any ice-surges are not likely to

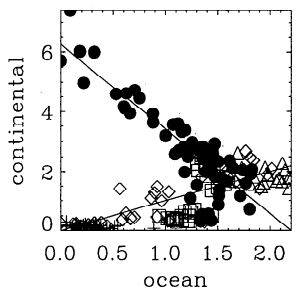

Figure 3. Scatter diagram for the continental and ocean source vectors, with symbol coding as follows; region 1 - crosses, region 2 - open diamonds, region 3 - open triangles, region 4 - filled dots, region 5 - open squares. This reveals a clearly different behaviour in region 4 than in all other regions.

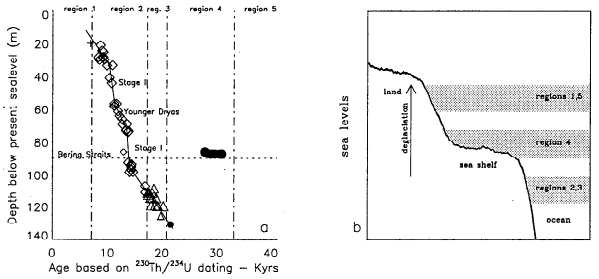

Figure 4. (a) Sea level data obtained from a Barbados coral core [*Fairbanks* 1990; *Bard et al* 1990]. Boxes indicate points dated using the $^{230}Th/^{234}U$ procedure, while diamonds were originally dated with ^{14}C methods and have been converted to the ^{230}Th/^{234}U ages using a regressional polynomial relationship [*Bard* 1992]. The highlighted temporal regions have been adjusted to the new timescale as above, and are equivalent to those in previous figures. Stage I and Stage II refer to meltwater events related to periods of accelerated deglaciation. (b) Schematic of changing sea level effects during ice-surge events over the different temporal regions.

have been strong enough to block them off as sources through flooding. This would allow for vegetation to take hold and render the region inactive as a source area. Rising sea levels during deglaciation would then remove them from the system permanently. This proposed mechanism is shown schematically in figure 4(b) which can be compared with sea level changes over the past 32 Kyrs taken from the Barbados coral core (figure 4(a)). Although the resolution is not high, comparison with the current average sea level around the Bering Straight ($< 100m$) suggests that such a mechanism is feasible.

Based on the assumption that source types maintain a constant relative abundance in time, it has been possible to reconstruct a picture of the large scale climate dynamics over the past 41 Kyrs. In particular the analysis has separated components directly correlated with terrestrial dusts during the build up to LGM. This has enabled us to contribute to the reconstruction of climatic conditions over this period, partly explaining the massive increase and dramatic fluctuations of continental acrosol in Greenland by a magnitudc of upto 100 over present day values.

Acknowledgments. Thanks to NCAR for hospitality and J.S. Pedersen for valuable discussions. The work was partly funded by the Carlsberg Foundation and partly by the Environment Program of the Commission for the European Communities.

References

Bales R.C. & Wolff E.W., Interpreting Natural Climate signals in ice-cores, *EOS*, 47, 477, 1995.

Bard E., Hamelin, B., Fairbanks, R. G., Zindler, A., Calibration of the ^{14}C timescale over the past 30 000 years using mass spectrometric U-Th ages from Barbados corals, *Nature*, 345, 405-409, 1990.

Bard E. *4th International Congress on Paleoceanography*, Kiel, 1992.

Biscaye P.E. et al, Asian provenance of glacial dust (stage 2) in the GISP2 ice core, Summit, Greenland, *JGR - special issue* (in press).

Bond G.C. & Lotti R., Iceberg discharges into the North Atlantic on millenial time scales dusring the last Glaciation, *Science*, 267, 1005-1010, 1995.

Clausen H.B. et al, 1250 years of global volcanism as revealed by central Greenland ice cores, in *Ice CoreStudies of Global Biogeochemical Cycles*, edited by Delmas R.J., pp 175-194, NATO ASI Series, 1993.

CLIMAP Project Members, *ibid.* 191, 1131, 1976.

Dansgaard W. et al., Evidence for general instability of past climate from a 250-kyr ice-core record,*Nature*, 364, 218-220, 1993.

Dansgaard W., White J.W.C., Johnsen S.J., The abrupt termination of the Younger Dryas climate event, *Nature*, 339, 532-533, 1989.

Ditlevsen P.D. & Marsh N.D., new method for identification of sources for chemical time series, and its application to the GISP ice-core record, *JGR* (in review).

Fairbanks R.G., The age and origin of the Younger Dryas climate event in Greenland ice-cores, *Paleoceanography*, 5, No. 6, 937-948, 1990.

GRIP members, Climate instability during the last interglacial period recorded in the GRIP ice-core, *Nature*, 364, 203-207, 1993.

Grootes et al, Comparison of oxygen isotope records from the GISP2 and GRIP Greenland ice cores, *Nature*, 366, 552-554, 1993.

Hammer C.U. et al, Continuous impurity analysis along the Dye 3 deep core, *Greenland Ice Core* edited by Langway C.C., Oeschger H., Dansgaard W.) Am. geophys. Monogr. 33, 1985.

Hansson M.E., The Renland ice core. A Northern Hemisphere record of aerosol composition over 120000 years, *Tellus*, 46B, 390-418, 1994.

Heinrich H., Origin and consequences of cyclic ice rafting in the northeast Atlantic Ocean during the past 130 000 years, *Quat. Res. N. Y.*, 29, 143-152, 1988.

Holland H.D. *The Chemistry of Atmosphere and Oceans*, Chap. 5, pp 153-249, Wiley Science, New York, 1978.

Johnsen S. J., Dansgaard W. & White J., The origin of Arctic precipitation under present and glacial conditions, *Tellus*, 41B(4), 452-468, 1989.

Marsh N.D. & Ditlevsen P.D., Observation of Atmospheric and climate dynamics from high resolution ice-core record of a passive tracer over the last Glaciation, *JGR*, (in press).

Mayewski P. et al, Changes in atmospheric circulation and ocean cover over the North Atlantic during the last 41 000 years, *Science*, 263, 1747-1751, 1994.

Mayewski P. et al, The atmosphere during the Younger Dryas, *Science*, 261, 195-197, 1993.

Meese D. et al, Preliminary depth-age scale of the GISP2 ice core, *CRREL Special Report*, 94-1, 1994.

Peltier W.R., Ice age paleotopography, *Science*, 265, 195-201, 1994.

Stuiver M. et al, The GISP2 delta 18O climate record of the past 16 500 years and the role of the sun, ocean, and volcanoes, *Quat. Res.*, 44, 341-354, 1995.

Wolff E.W. in Ice Core Studies of Global Biogeochemical Cycles (ed. Delmas R.J.) pp 225-240, NATO ASI Series, 1993.

N.D. Marsh & P.D. Ditlevsen, Department of Geophysics, Niels Bohr Institute, University of Copenhagen, Juliane Maries Vej 30, DK-2100 Copenhagen OE, Denmark. (e-mail: ndm@gfy.ku.dk; pditlev@gfy.dk.ku)

(Received November 20, 1996; revised February 10, 1997; accepted February 10, 1997.)